Supplementary Information (SI) for ChemComm.
This journal is © The Royal Society of Chemistry 2026

Electronic Supplementary Information

The Construction of Stable Cu-O-Fe Bridging Structure for Highly Efficient Electrocatalytic Nitrate Reduction to Ammonia

Zhengguo Qu,[a,b] Shengbo Zhang,*[c] Jiheng Zhu,[c] Zhixian Mao,[a] Min Liu,[a] Pan Gao,[b] Haoran Wu,[a] Jian Ma,[a] Qiong Tang,*[b] Tongfei Shi*[a]

[a] Institute of Solid State Physics, HFIPS, Chinese Academy of Sciences, Hefei 230031, China

[b] School of Physics，Hefei University of Technology, Hefei 230009, Anhui, China

[c] Macao Institute of Materials Science and Engineering (MIMSE), Faculty of Innovation Engineering, Macau University of Science and Technology, Taipa, Macao 999078, China.

* Corresponding author: E-mail: tfshi@issp.ac.cn; shbzhang@issp.ac.cn; jennytq@hfut.edu.cn

1. Experimental Section

1.1. Chemicals and materials

Copper foam (CF) were purchased from Kunshan Guangjiayuan New Materials Co.,Ltd.$Fe(NO_3)_3{\cdot}9H_2O$, $CuSO_4{\cdot}_5H_2O$, KNO_3 (99.0%), sodium nitroferricyanide(III) dehydrate ($C_5FeN_6Na_2O{\cdot}2H_2O$, 99.0%), sodium citrate ($C_6H_5Na_3O_7{\cdot}2H_2O$, 99.0%), KOH (96.0%), ethylene glycol ($(CH_2OH)_2$, 99.0%), glycolic acid ($C_2H_4O_3$, 99.0%), salicylic acid ($C_7H_6O_3$, 99.5%), NaClO (available chlorine ≥ 5.0%), NH_4Cl (99.5%), thiosemicarbazide (CH_5N_3S, 99.0%), p-aminobenzenesuifonamide ($NH_2C_6H_4SO_2NH_2$, 95.0%), N-(1-naphthyl) ethylenediamine dihydrochloride ($C_{10}H_7NHC_2H_4NH_2{\cdot}2HCl$, 95.0%), $^{15}KNO_3$ (AR), $^{14}NH_4Cl$ (AR), $^{15}NH_4Cl$ (AR), were purchased from Shanghai Aladdin Biochemical Technology Co., Ltd. Shanghai. All solutions were prepared using deionized water (Millipore Corp., 18.2 MΩ cm). Commercial carbon paper (CP, HCP030N) was purchased from Shanghai Hesen Electric Co. Ltd.

1.2. Synthesis of CuFe-CF, Cu-CF and Fe-CF

The CuFe-CF catalyst was fabricated via a facile, one-step electrodeposition process within a three-electrode cell. Prior to deposition, a piece of copper foam (CF, 2 × 1.5 cm) was ultrasonically cleaned in 1 M HCl for 10 min to remove surface oxides, followed by thorough rinsing with deionized water and absolute ethanol. Using the treated CF as the working electrode (WE), Ag/AgCl as the reference electrode (RE), and a platinum mesh as the counter electrode (CE), electrodeposition was performed at -1.2 V *vs*. Ag/AgCl for durations of 10, 15, and 20 minutes in a single-compartment cell. The deposition electrolyte consisted of 50 mM $CuSO_4{\cdot}5H_2O$ and 50 mM

$Fe(NO_3)_3 \cdot 9H_2O$. Post-deposition, samples were rinsed multiple times with deionized water and ethanol and subsequently dried under vacuum at 60 ℃ for 2 h.

The preparation methods for Cu-CF and Fe-CF were similar to that of CuFe-CF, with the only difference being that the precursor solution contained solely Cu^{2+} or Fe^{3+}, respectively, for the synthesis of Cu-CF and Fe-CF.

1.3. Material characterization

The scanning electron microscopy (SEM) images were obtained using SU8020 (Hitachi, Japan). The transmission electron microscopy (TEM) images were obtained using JEMARM 200F. The aberration-corrected high-angle annular dark-field scanning transmission electron microscopy (HAADF-STEM) measurements andenergy-dispersive X-ray (EDX) spectroscopy were performed using JEMARM200F. X-ray diffraction (XRD) patterns were acquired using Philips X'pert PRO with Cu Ka radiation (λ = 1.5418 Å) at 40 kV and 40 mA. Nitrogen adsorptiondesorption isotherms were measured using Autosorb-iQ-Cx. X-ray photoelectron spectroscopy (XPS) analysis was performed on an ESCALAB 250 X-ray photoelectron spectrometer (Thermo, America). Electrochemical measurements All the electrochemical measurements were performed on a CHI 660E electrochemical workstation (CH Instrumental Corporation, Shanghai, China) using an H-type cell, which was separated by a Nafion 211 proton exchange membrane. The Nafion 211 membrane was treated at 80 ℃ in H_2O_2 (5 wt.%) and 0.5 M H_2SO_4 aqueous solution in turn to protonate and then rinsed with deionized water before use. The saturated Ag/AgCl electrode was used as the reference electrode and a platinum mesh was used as the counter electrode. Before

use, the working electrode was activated in 0.1 M KOH + 0.25 M KNO_3 solution. Unless otherwise stated, all experiments were performed in 0.1 M KOH + 0.25 M KNO_3 solution. All measured potentials versus Ag/AgCl were transformed into the potentials versus reversible hydrogen electrode (RHE) according to the following equation:

$$E_{RHE} = E_{Ag/AgCl} + 0.059\,pH + E^{0}_{Ag/AgCl}$$

where the $E_{Ag/AgCl}$ is the equilibrium potential under standard conditions and $E^{0}_{Ag/AgCl}$ = 0.197 V versus RHE at 25℃.

1.4. Determination of ammonia.

The concentration of the produced ammonia was detected by the indophenol blue method.[1] In detail, taken 100 μL of electrolyte in a cathode cell after 2 h electrocatalysis, and then added 9900 μL of deionized water in a 15 ml colorimetric tube. Subsequently, 500 μL of coloring agent (composed of 10 g salicylic acid, 10g sodium citrate, 55 ml 2.0 M sodium hydroxide with deionized water in 200 ml solution), 100 μL of oxidizing solution (containing 5ml sodium hypochlorite and 45ml 2.0 M sodium hydroxide in 50 ml solution), and 100 μL of catalyst solution (1.0 g $Na_2[Fe(CN)_5NO]\cdot 2H_2O$ diluted to 100 mL with deionized water) were added to the measured sample solution in turn. After the color development for 1h at room temperature, the absorbance measurements were performed by UV-Vis spectrophotometer at a wavelength of 697.5 nm. The obtained calibration curve was used to calculate the ammonia concentration.

1.5. Determination of nitrite.

The produced nitrite in the electrolyte was detected by the Griess method.[2] In detail, the N-(1-naphthyl) ethylenediamine dihydrochloride (1 g), sulfonamide (20 g) and H_3PO_4 (50 mL, 85%) were dissolved in 250 ml of deionized water and then set the

mixture to 500 ml volumetric flask to form the Griess reagent. Added 1 ml of reacted electrolyte with 9 ml of deionized water into a 15 ml colorimetric tube then mixed with 200 μL of Griess reagent and placed for 20 min at room temperature. UV-vis spectrophotometer was used to measure the absorbance of the generated nitrite at the wavelength of 540 nm. Then the concentration of NO_2^- was obtained by the calibration curve.

1.6. Calculation of NtrRR Performance

R_{NH_3}, FE and S_{NH_3} are calculated by the following formulas:

$$Yield\ Rate_{NH3}(\mu g\ h^{-1}\ mg_{cat.}^{-1}) = \frac{C_{NH3}(\mu g\ mL^{-1}) \times V(mL)}{t(h) \times m_{cat.}(mg)}$$

$$FE\ (\%) = \frac{8 \times n_{NH_3}(mol) \times F(C\ mol^{-1})}{Q\ (C)} \times 100\%$$

$$S_{NH_3}(\%) = \frac{\Delta C_{N\text{-}NH_3}}{\Delta C_{N\text{-}NH_3} + \Delta C_{N\text{-}NO_2^-}} \times 100\%$$

C_{NH_3} is the concentration of produced NH_3 and V is the volume of electrolyte. t is the electrolysis time, S is the area of the loaded electrocatalyst, F is the faradaic constant (96485 C mol^{-1}) and Q is the total charge transferred during electrolysis. C_{N-NH_3} is the concentration of produced $N-NH_3$ and $N-NO_2^-$ is the concentration of produced -NO_2^-.

$R_{NO_2^-}$ and FE are calculated by the following equations:

$$Yield\ Rate_{NO_2^-}(\mu g\ h^{-1}\ mg_{cat.}) = \frac{C_{NO_2^-}(\mu g\ mL^{-1}) \times V(mL)}{t(h) \times m_{cat.}(mg)}$$

$$FE\ (\%) = \frac{2 \times n_{NO_2^-}(mol) \times F(C\ mol^{-1})}{Q\ (C)} \times 100\%$$

where, $C_{NO_2^-}$ and V are the measured NO_2^- concentration and the electrolyte solution volume, respectively, t is the electrolysis period and $m_{cat.}$ is the amount of the

loaded electrocatalyst, F is the faradaic constant (96485 C mol^{-1}) and Q is the total charge transferred during electrolysis period.

1.7. ^{15}N Isotope Labelling Experiments

For quality assurance required, ^{15}N isotopic labelling experiments were conducted using 0.1 M KOH + 0.25 M $K^{15}NO_3$ as the electrolyte with identical experimental procedure as that of Ar-saturated 0.1 M KOH + 0.25 M $K^{14}NO_3$ experiments. For ^1H NMR method, D_2O (99.9 atom% D, Aladdin Biochemical Technology Co., Ltd. Shanghai) used as internal standard. The yielded $^{15}NH_3$ were analyzed by the ^1H NMR methods using Bruker Avance-400 MHZ.

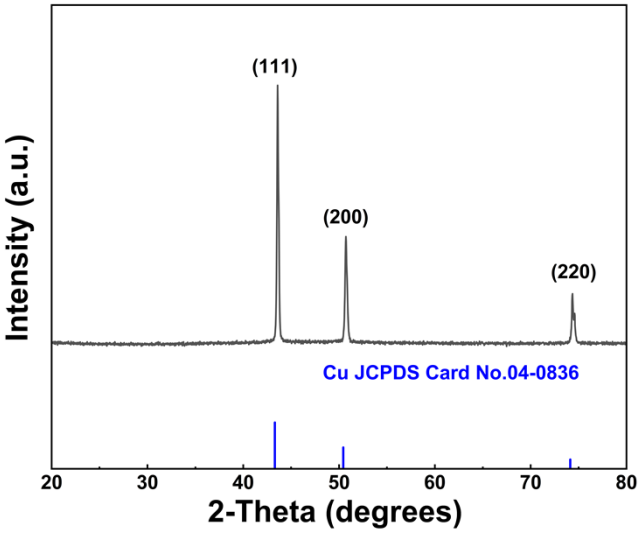

Fig. S1 XRD pattern of CuFe-CF.

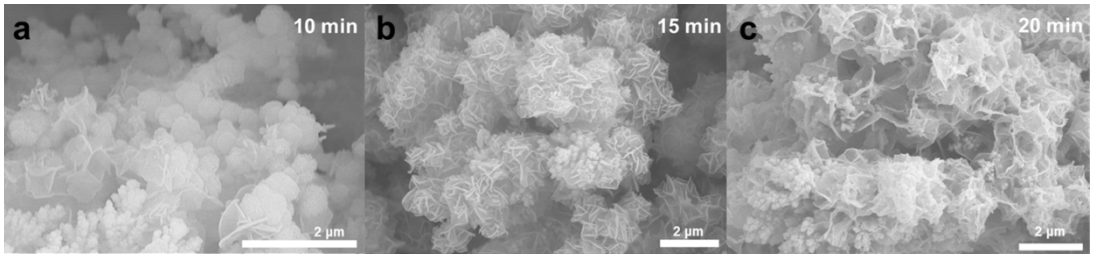

Fig. S2 Scanning images of CuFe-CF deposited at different times by electrodeposition 10, 15 and 20 min.

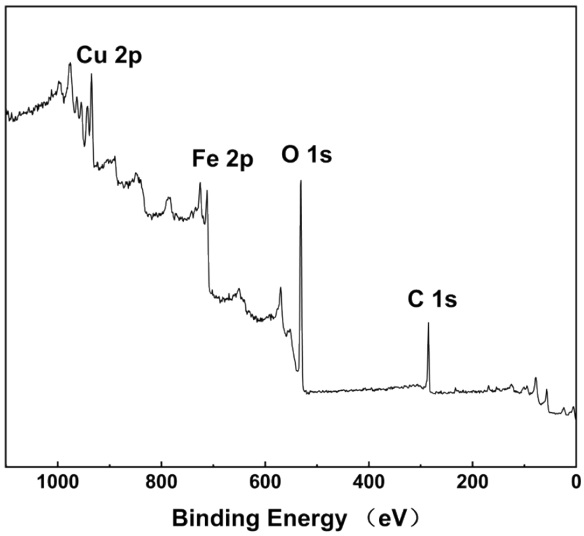

Fig. S3 Surface survey XPS spectra of the CuFe-CF sample.

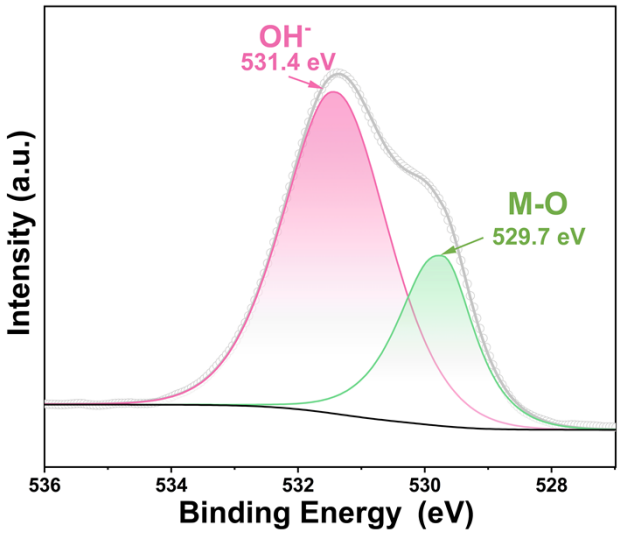

Fig. S4 The high-resolution O 1s spectrum of the CuFe-CF.

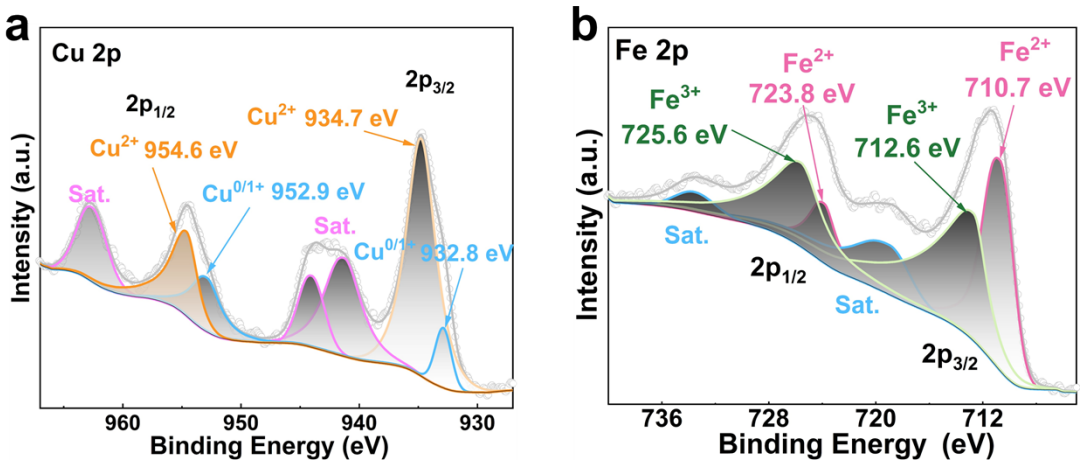

Fig. S5 The high-resolution (a) Cu 2p and Fe 2p spectra of the CuFe-CF.

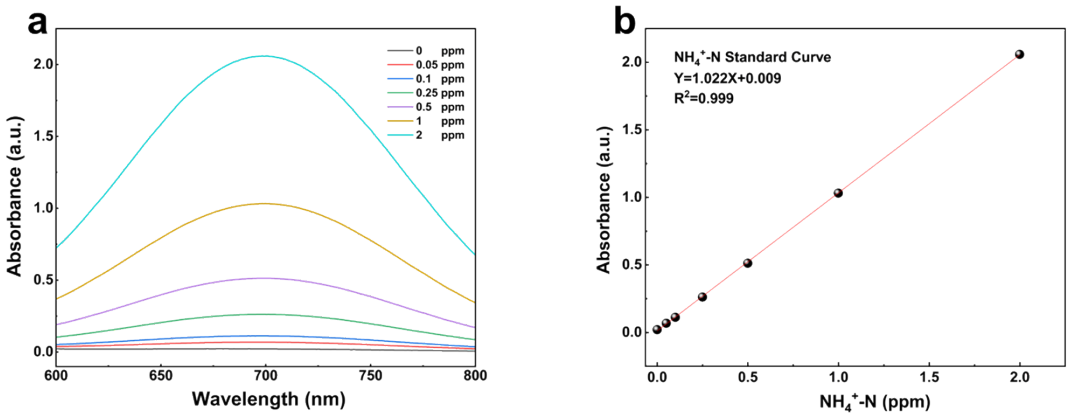

Fig. S6 (a) UV-Vis absorption spectra obtained from the solutions with different NH_4^+-N concentrations (0, 0.05, 0.1, 0.25, 0.5, 1.0 and 2.0 ppm). (b) Calibration curve used to determine NH_4^+-N concentration.

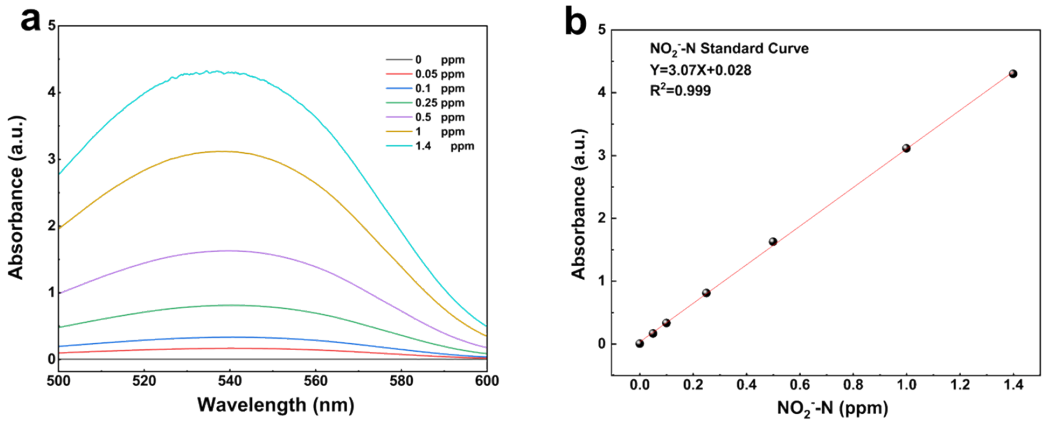

Fig. S7 (a) UV-Vis absorption spectra of various NO_2^--N concentrations (0, 0.05, 0.1, 0.25, 0.5, 1.0 and 1.4 ppm). (b) The calibration curve used for calculation of NO_2^--N concentrations.

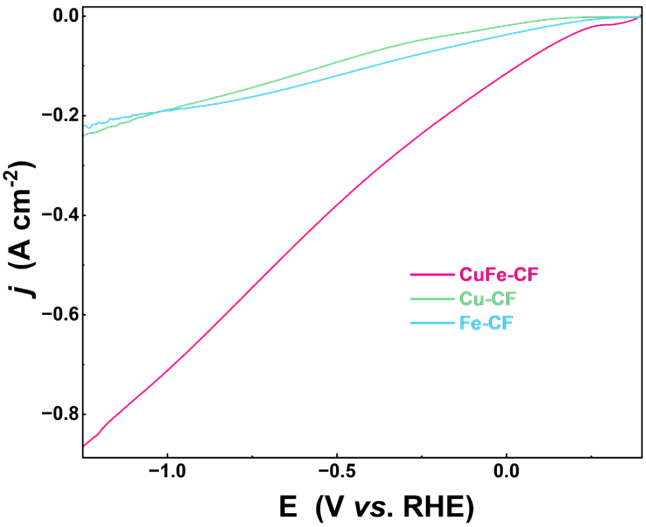

Fig. S8 LSV curves of the CuFe-CF, Cu-CF and Fe-CF catalyst in 0.1 M KOH and 0.1 M KOH + 0.25 M KNO_3 solutions.

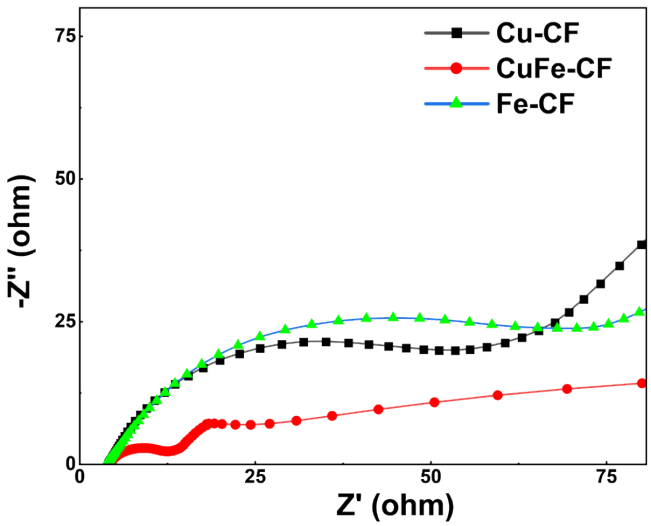

Fig. S9 EIS Nyquist plots (amplitude: 5 mV, open-circuit potential, frequency range: 100 kHz-0.01 Hz) of the pristine CuFe-CF, Cu-CF, and Fe-CF electrocatalysts.

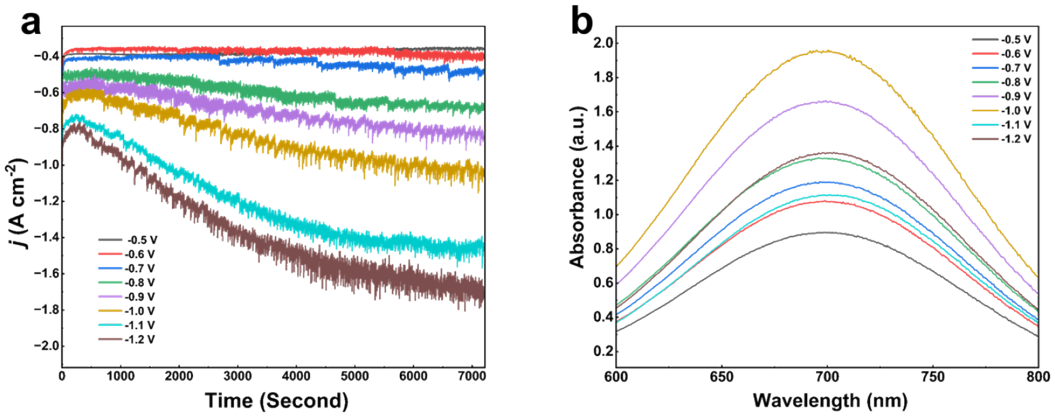

Fig. S10 (a) The j-t curves at different potentials in 0.1 M KOH + 0.25 M KNO_3 electrolyte over a 2 h period. (b) UV-Vis absorption spectra of the corresponding samples.

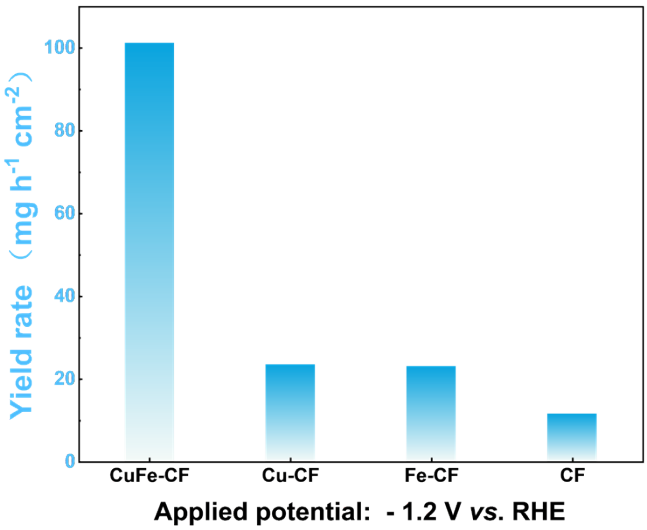

Fig. S11 Comparison of NH_3 yield rate of CuFe-CF, Cu-CF and Fe-CF.

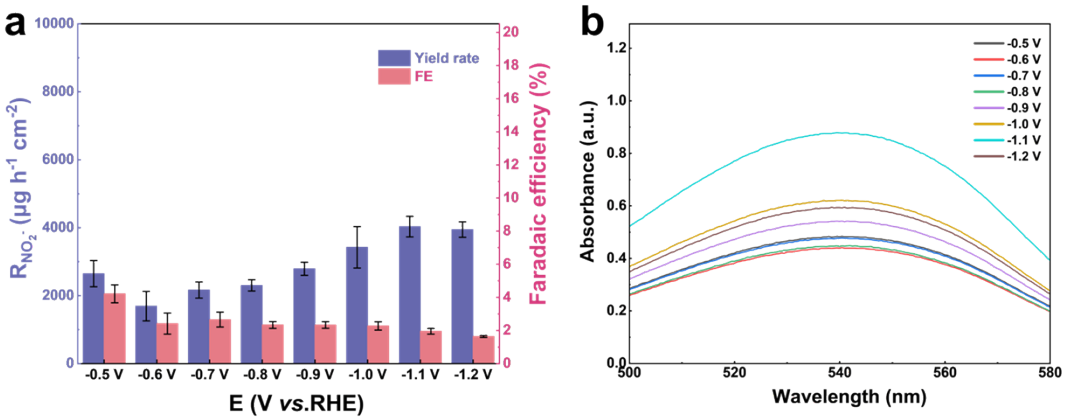

Fig. S12 (a) The yield rate and FE of NO_2^- in different potentials between -0.5 to -1.2 V (vs. RHE). (b) UV-Vis absorption spectra of the corresponding samples.

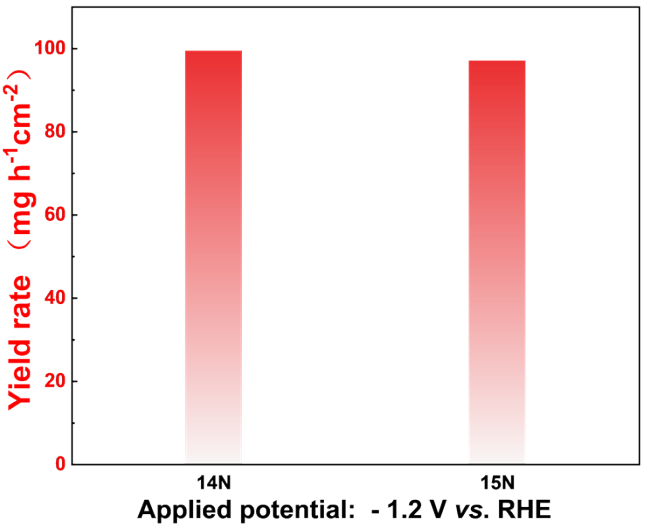

Fig. S13 Comparison of NH_3 yield rate from CuFe-CF using $^{14}NO_3^-$ and $^{15}NO_3^-$ as nitrogen source, respectively.

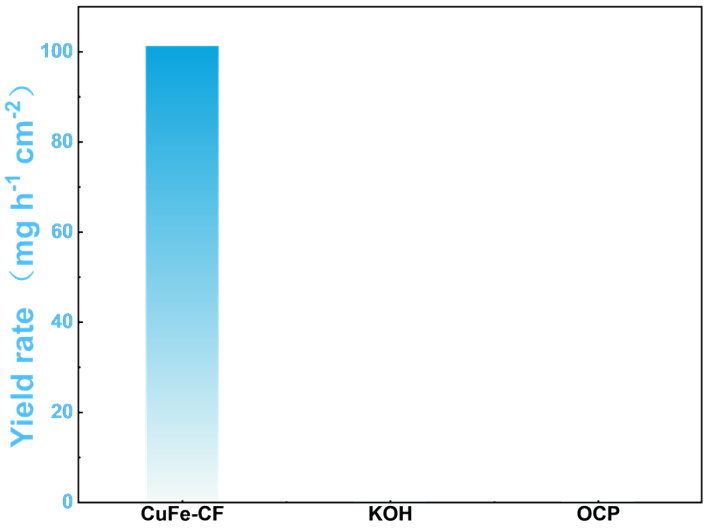

Fig. S14 NH_3 yield rate contrast experiments with different conditions 0.1 M KOH, OCP, CP and CuFe-CF at −1.2 V (*vs*. RHE) for 2 h.

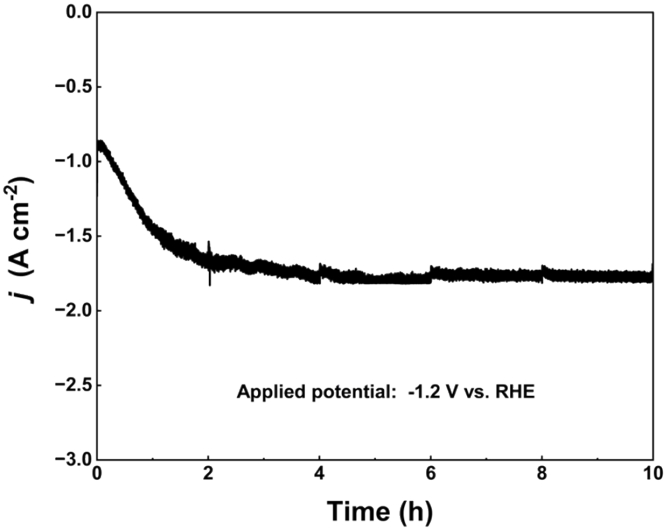

Fig. S15 Long-time stability test of CuFe-CF at −1.2 V (*vs*. RHE).

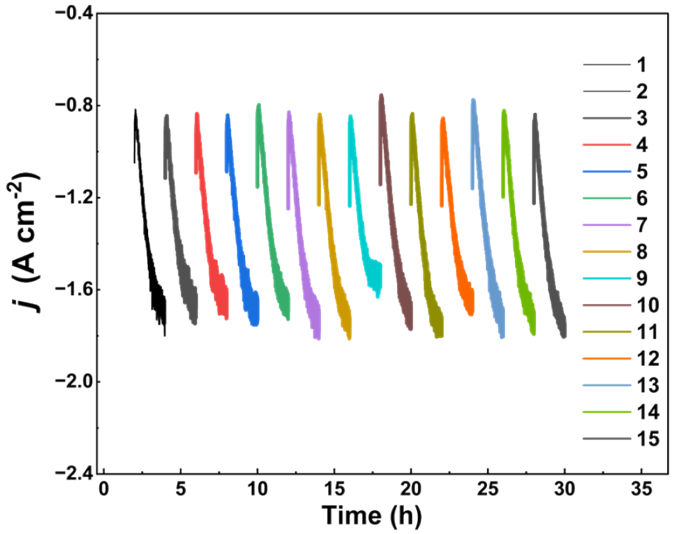

Fig. S16 Cycling stability test of CuFe-CF at −1.2 V (*vs*. RHE) for 15 cycles with 2.0 h NtrRR period per cycle.

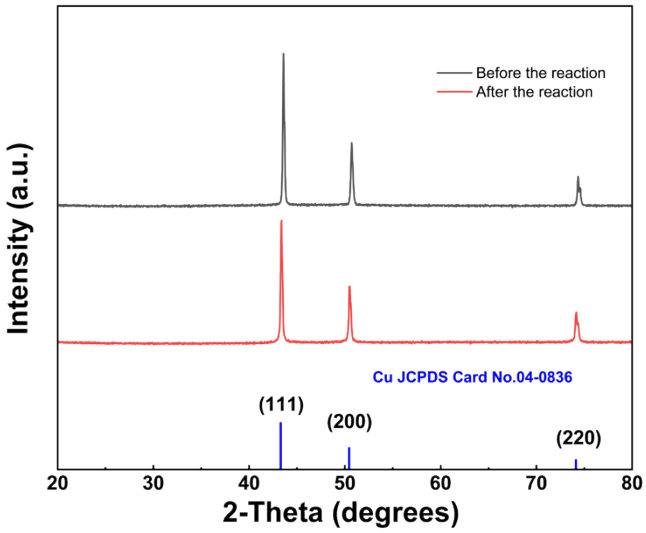

Fig. S17 XRD patterns of CuFe-CF after 15 NtrRR recycles.

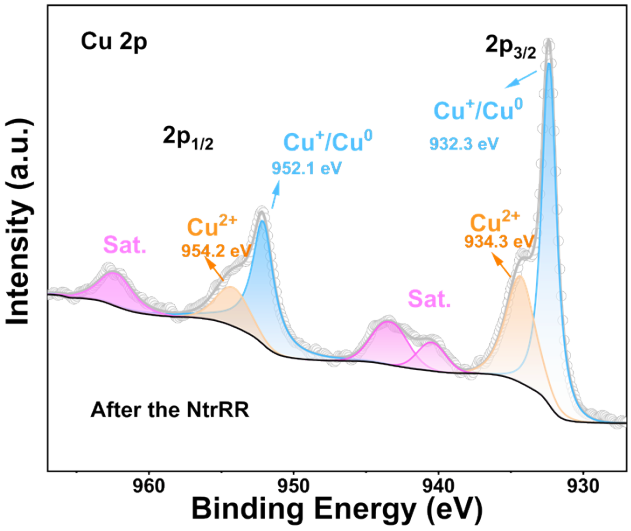

Fig. S18 High-resolution XPS spectra of Cu 2p of CuFe-CF after NtrRR.

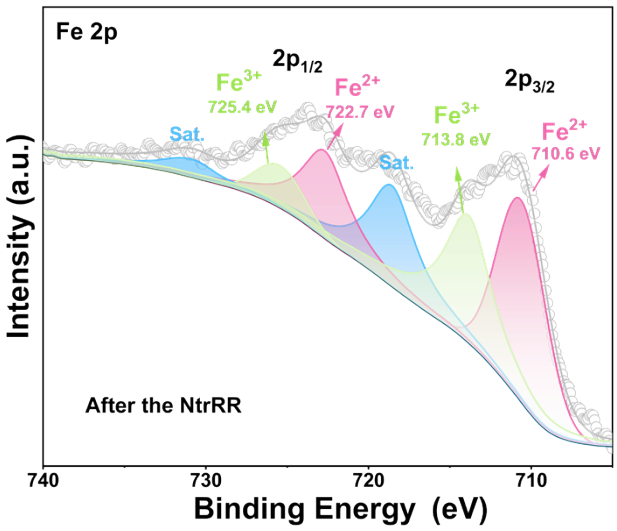

Fig. S19 High-resolution XPS spectra of Fe 2p of CuFe-CF after NtrRR.

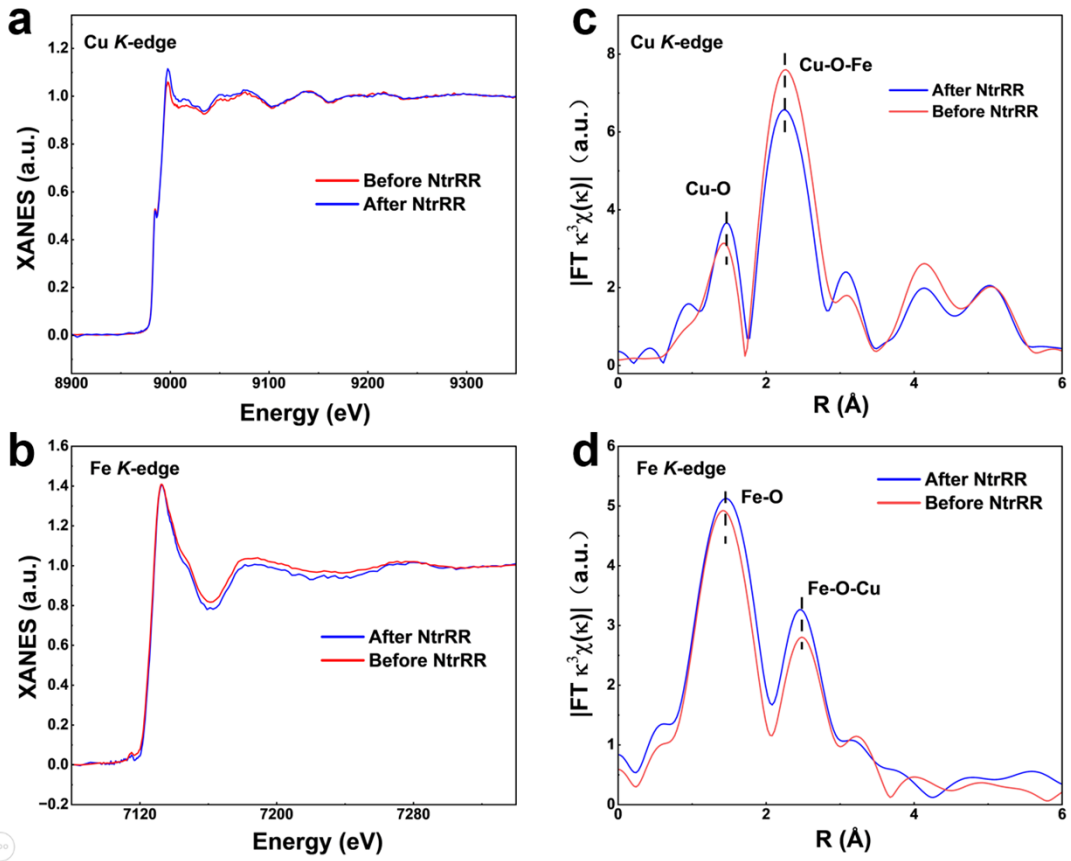

Fig. S20 (a) Cu *K*-edge and (b) Fe *K*-edge XANES spectra of CuFe-CF before and after NtrRR. (c) Cu *K*-edge and (d) Fe *K*-edge k^3-weighted FT-EXAFS spectra of CuFe-CF before and after NtrRR.

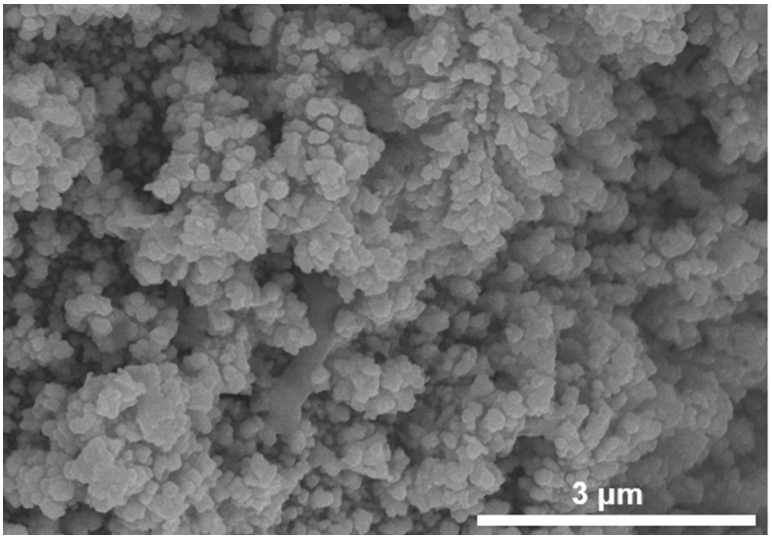

Fig. S21 SEM image of CuFe-CF after 15 NtrRR recycles.

Table S1. Comparison of NtrRR performance between CuFe-CF catalyst and others electrocatalysts recently-reported.

Catalyst	NO_3^- concentration	Electrolyte	NH_3 yield rate	FE(%)
RuO_2/Co_3O_4[3]	1 M	1 M KOH	35.9 (mg h^{-1} cm^{-2})	98.1 (-0.3 V *vs*. RHE)
NiTP−CoTAPP[4]	0.5 M	-	2.723 (mg h^{-1} $mg_{cat.}^{-1}$)	85.6 (-1.0 V *vs*. RHE)
Ni_{35}/NC-sd[5]	0.3 M	0.5 M Na_2SO_4	5.1 (mg h^{-1} cm^{-2})	99 (-0.5 V *vs*. RHE)
Fe SAC[6]	0.5 M	0.1 M Na_2SO_4	7.8 (mg h^{-1} cm^{-2})	74.9 (-0.85 V *vs*. RHE)
CNS-CoP[7]	1 M	1 M KOH	55.7 (mg h^{-1} cm^{-2})	90.5 (-1.03 V *vs*. RHE)
Cu-Cu_2O/Ni_2P[8]	0.1 M	0.1 M PBS	10.636 (mg h^{-1} cm^{-2})	96.4 (-1.0 V *vs*. RHE)
Si/I-NiO@CC[9]	0.5 M	0.1M K_2SO_4	10.6 (mg h^{-1} cm^{-2})	96.8 (-0.3 V *vs*. RHE)
Ru-ST-12[10]	1 M	1 M KOH	19.9 (mg h^{-1} cm^{-2})	98.5 (-0.6 V *vs*. RHE)
Pd-NDs/Zr-MOF[11]	1 M	0.1M $HClO_4$	0.28 (mg h^{-1} $mg_{cat.}^{-1}$)	58.1 (-1.3 V *vs*. RHE)
Cu/CuAu[12]	1 M	1 M KOH	1.7 (mg h^{-1} cm^{-2})	85.5 (-0.6 V *vs*. RHE)
Cu–CoO@CNT[13]	0.25 M	0.1 M KOH	83.2 (mg h^{-1} $mg_{cat.}^{-1}$)	84.8 (-0.9 V *vs*. RHE)
This work	0.25 M	0.1 M KOH	102.3 (mg h^{-1} cm^{-2})	92.3 (-1.2 V *vs*. RHE)

References

1 D. Zhu, L. Zhang, R. E. Ruther and R. J. Hamers, *Nature Mater*, 2013, **12**, 836–841.

2 Y. Xin, S. Zhang, J. Liu, Y. Jiang, Y. Zhang, G. Wang and H. Zhang, *Inorg. Chem. Front.*, 2024, **11**, 8371–8376.

3 A. Zhu, H. Liu, L. Qiao, B. Liu, K. Liu, C. Luan, K. Liu, Y. Zhou, D. Lin, G. Gan, J. Li, G. Hong and W. Zhang, *Adv. Mater.*, 2026, **38**, e15346.

4 Z. Zhang, M. Wang, H. Xing, X. Zhou, L. Gao, S. Chen, Y. Chen, H. Xu, W. Li, S. Yuan, C. Li, Z. Jin and J. Zuo, *Angew Chem. Int. Ed.*, 2025, **64**, e202505580.

5 P. Gao, Z. Xue, S. Zhang, D. Xu, G. Zhai, Q. Li, J. Chen and X. Li, *Angew Chem. Int. Ed.*, 2021, **60**, 20711–20716.

6 Z. Y. Wu, M. Karamad, X. Yong, Q. Huang, D. A. Cullen, P. Zhu, C. Xia, Q. Xiao, M. Shakouri, F. Y. Chen, J. Y. Kim, Y. Xia, K. Heck, Y. Hu, M. S. Wong, Q. Li, I. Gates, S. Siahrostami and H. Wang, *Nat. Commun.*, 2021, **12**, 2870.

7 K. Fan, W. Xie, J. Li, Y. Sun, P. Xu, Y. Tang, Z. Li and M. Shao, *Nat Commun*, 2022, **13**, 7958.

8 H. Zhao, P. Liu, X. Cheng, C. Fan, J. Liu, D. Kan and Y. Wang, *Adv. Funct. Materials.*, 2025, **35**, 2425459.

9 C. Feng, K. Bo, J. Wan, H. Zhang and Y. Wang, *Angew Chem. Int. Ed.*, 2025, **64**, e202505211.

10 J. Li, G. Zhan, J. Yang, F. Quan, C. Mao, Y. Liu, B. Wang, F. Lei, L. Li, A. W. M. Chan, L. Xu, Y. Shi, Y. Du, W. Hao, P. K. Wong, J. Wang, S. X. Dou, L. Zhang and J. C. Yu, *J. Am. Chem. Soc.*, 2020, **142**, 7036–7046.

11 M. Jiang, J. Su, X. Song, P. Zhang, M. Zhu, L. Qin, Z. Tie, J. L. Zuo and Z. Jin, *Nano Lett.*, 2022, **22**, 2529–2537.

12 Q. Gao, B. Yao, H. S. Pillai, W. Zang, X. Han, Y. Liu, S. W. Yu, Z. Yan, B. Min, S. Zhang, H. Zhou, L. Ma, H. Xin, Q. He and H. Zhu, *Nat. Synth.*, 2023, **2**, 624–634.

13 Z. Qu, S. Zhang, Z. Mao, M. Liu, L. Zhou, H. Zhang, F. Song, Z. Li, Q. Tang and T. Shi, *Chem. Commun.*, 2026, **62**, 3555–3559.